



# Coordinated design of PSS and multiple FACTS devices based on the PSO-GA algorithm to improve the stability of wind–PV–thermal-bundled power system

Ping He<sup>1</sup> · Zhiwen Pan<sup>1</sup> · Jiale Fan<sup>1</sup> · Yukun Tao<sup>1</sup> · Mingyang Wang<sup>1</sup>

Received: 20 March 2023 / Accepted: 20 September 2023 / Published online: 13 October 2023  
© The Author(s), under exclusive licence to Springer-Verlag GmbH Germany, part of Springer Nature 2023

## Abstract

In order to realize the coordinated design of multiple flexible AC transmission systems (FACTS) devices in the wind–PV–thermal-bundled (WPTB) power transmission system to suppress the low-frequency oscillation (LFO) of the system, in this paper, the static synchronous compensator (STATCOM) and the static synchronous series compensator (SSSC) with additional power oscillation damping controller (PODC) are designed based on the tie line transmission power signal to enhance the improvement effect of FACTS devices on system stability. The objective function is constructed by considering the transient voltage stability of the WPTB power transmission system, the real part of the eigenvalues and damping level of the LFO modes. And the coordinated and optimized design of power system stabilizer (PSS), SSSC-PODC and STATCOM-PODC is performed by the hybrid particle swarm optimization algorithm and genetic algorithm (PSO-GA) and pattern analysis theory of LFO. Finally, it is verified that the design can give full play to the effect of different controllers and significantly improve the damping ratio of the oscillation mode between regions through the simulation under the output variation of the new energy unit and the transmission power variation of the liaison line. When the fault occurs, the amplitude of oscillation and the time required to recover stability of the system decrease obviously, which enhances the dynamic stability of the system.

**Keywords** WPTB power transmission system · STATCOM-PODC · SSSC-PODC · PSO-GA · LFO · Voltage stability

## 1 Introduction

The large-scale application of new energy generation represented by wind power and photovoltaic (PV) power generation can optimize the energy structure and improve the natural environment [1, 2], which is of great significance

to the achievement of China's "30–60" carbon peak carbon neutral goal [3, 4]. Thanks to the wind–PV–thermal-bundled (WPTB) power transmission system [5, 6], the development of large-scale new energy bases and energy delivery in north-east, north and northwest China have become more efficient. At the same time, the application of the system has greatly expanded the scope of new energy consumption and can well meet the electricity demand of users in the eastern and central regions. At present, it has become an important way for large-scale new energy bases in China to realize efficient power transportation [7].

However, the wind turbines and PV plants connected to the conventional power system will significantly affect the damping ratio of the system and affect the damping characteristics of the system. Consequently, the power system becomes highly susceptible to low-frequency oscillations (LFOs) as a result of reduced damping when disturbances occur. Wind power and PV power generation have a certain volatility, which will also increase the probability of unbalanced tides in the power system, resulting in more oscillation problems

✉ Ping He  
hplkz@126.com  
Zhiwen Pan  
1120441179@qq.com  
Jiale Fan  
fanjiale@zzuli.edu.cn  
Yukun Tao  
395391035@qq.com  
Mingyang Wang  
2394081906@qq.com

<sup>1</sup> College of Electrical and Information Engineering, Zhengzhou University of Light Industry, Zhengzhou 450002, Henan Province, China

[8, 9]. In addition, the interaction between new energy units and traditional thermal generating units will also affect the damping torque and LFO characteristics of the system, so that the interconnected power grid is prone to LFO and inter-area LFO due to the reduction in the damping, thus affecting the transmission capacity between the connected lines of the interconnected system. For large-scale interconnected systems, the transmission capacity and stability of tie lines are crucial, and serious LFOs can even lead to grid disconnection of the power system, limiting the grid-connected scale of new energy generation. It can be seen that the stability problem is prominent in the new energy power system.

Power system stabilizer (PSS) installed on the excitation system of synchronous thermal generating units can effectively suppress the LFO of traditional power system, but in present-day power systems, because of the access of new energy sources, inter-area oscillations are difficult to suppress effectively under certain operating conditions using only PSS control, so other more effective measures are needed to suppress LFOs and simultaneously improve the system's dynamic stability [10]. Flexible AC transmission systems (FACTS) devices have found application in actual power system as power electronics have advanced. FACTS can accomplish continuous regulation and control of system voltage, line impedance, phase angle, both reactive and active power which can increase the transmission distance of transmission lines and enhance the stability of the system [11, 12]. However, with the increase in the proportion of renewable energy in the power system, a single FACTS device cannot improve the damping characteristics of the power system to ensure the stable operation of the system. With the in-depth study, the interaction and coordinated design between multiple controllers have become a research hotspot of power systems. The combination of static synchronous compensator (STATCOM) and power oscillation damping controllers (PODC) is proposed in the literature [13] which can improve the stability of the 4-machine 2-area power system under various disturbance conditions. In the literature [14], the improvement effect of static synchronous series compensator (SSSC) on the system was analyzed in a power system containing wind power and fuel cells. The results showed that fuel cells and SSSC can enhance the damping properties and transient stability of the system. The literature [15] analyzed the effectiveness of thyristor-controlled series compensation (TCSC) and static var compensator (SVC) for the application to suppress the oscillations caused by the conventional power system connected to high-permeability wind power. The simulation results show that TCSC is more effective than SVC in improving system stability.

With the increasing number of controllers in the system, multiple controllers can indeed achieve fast control and improve system stability, but there are also adverse interactions between them, which may deteriorate the control effect

and even cause system instability. The literature [16] states that, considering the negative interactions of multiple FACTS devices in a multi-machine system, to achieve coordinated control of multiple FACTS devices, it is necessary that the controller parameters satisfy the coordinated operation conditions. A multi-objective multi-model system strategy based on Bilinear matrix inequality (BMI) is used in the literature [17] to coordinate the design of SVC and TCSC, and verifies the effectiveness of all methods in the 5-area 16-generator 68-bus system. The suggested controller shows high robustness against various system disturbances and different operating conditions, according to the time-domain simulation findings. The literature [18] verified through simulation that there is an unfavorable interaction between the PSS and the UPFC-PODC, and that the coordinated optimization of the parameters of the PSS and the UPFC-PODC by the steepest descent algorithm can reduce the system oscillation amplitude and improve the system stability. In the literature [19], the effects of PSS and SSSC on the stability of power systems connected to doubly fed induction generator (DFIG) were investigated, and an objective function related to the rotor speed deviation was designed to coordinate and optimize the compensation degree of SSSC and the gain of PSS. The results show that the oscillations of the system can be suppressed to the maximum extent by optimizing the controller parameters.

In summary, this paper considers the coordinated control of PSS, STATCOM-PODC and SSSC-PODC to enhance the damping characteristics of the WPTB power transmission system and suppress the LFO of the system. Firstly, the SSSC-PODC controller and STATCOM-PODC controller are designed based on the tie line transmission power signal. Secondly, the objective function is constructed by considering the system transient voltage stability, real part of the eigenvalues and damping level of the LFO modes. Thirdly, GA and PSO are relatively mature optimization algorithms, which are considered as the benchmark of intelligent optimization technology by most scholars. The standardization and generality of GA and PSO [20] are considered, and the advantages of both algorithms are combined. A hybrid algorithm based on PSO and GA is proposed as an optimization method to coordinate and tune the parameters of multiple controllers. The PSO-GA algorithm and pattern analysis theory are used to coordinate and optimize the design of PSS, SSSC-PODC and STATCOM-PODC to improve the LFO properties of the system. Finally, the effectiveness of the designed parameter optimization method is verified by simulating the IEEE 4-machine 2-area system under various operating conditions, including new energy unit output change and contact line transmission power change.

The main contributions are as follows:

- Through the cooperative control of PSS and multiple FACTS devices, the LFO of the WPTB power transmission system is effectively suppressed and the system stability is significantly improved.
- A coordinated optimization method for PSS and multi-FACTS devices is proposed, which ensures the coordinated operation capability of multiple controllers based on PSO-GA algorithm, and better solves the coordinated design and operation problems of PSS, STATCOM-PODC and SSSC-PODC.
- The performance of the proposed parameter optimization method is verified in a modified IEEE 4-machine 2-area system by dynamic time-domain simulation and eigenvalue analysis under different operating conditions. The simulation results show that the synergistic optimization of PSS, STATCOM-PODC and SSSC-PODC can give full play to the effects of different controllers and significantly improve the damping ratios of inter-area oscillation modes; the oscillation amplitude and the time required to restore stability of the system are significantly reduced when a fault comes, which enhances the dynamic stability of the system.

The following is a brief introduction to the rest of this paper. Section II describes the models of the WPTB power transmission system, the FACTS devices and PSS. In Section III, the objective function that integrates the transient voltage stability of the system, the real parts and damping ratios of the eigenvalues of the LFO modes of the system is designed. In Section IV, the PSO-GA-based parameter optimization model is proposed. Section V optimizes the parameters of PSS, STATCOM-PODC and SSSC-PODC using PSO-GA, and the effectiveness of the proposed parameter optimization method is fully verified by a large number of examples through a modified IEEE 4-machine 2-area system using eigenvalue analysis and dynamic time-domain simulation. Finally, some useful conclusions are obtained in Section VI.

## 2 System modeling

### 2.1 The model of WPTB power transmission system

Figure 1 illustrates the connection diagram for the power system with WPTB power.  $\Delta P_b + j\Delta Q_b$  is the electric power injected into the power system by the WPTB, and  $\Delta P_s + j\Delta Q_s$  is the electric power received by the receiving end.

The wind power generation system is composed of DFIG, which is the mainstream model widely used at present. The shafting transmission device is considered to adopt a two-mass model, and its mathematical model mainly includes induction generator, mechanical transmission part, wind

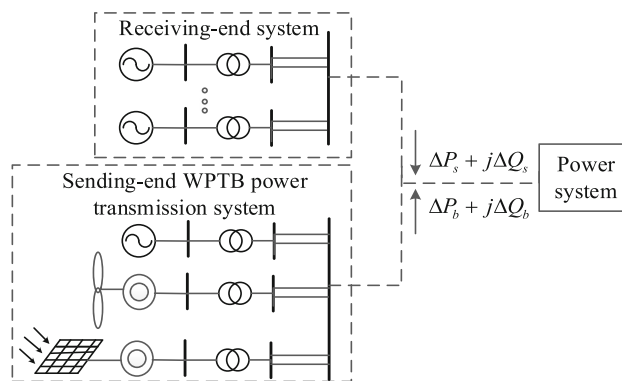


Fig. 1 Connection diagram of WPTB power transmission system

power model, wind speed model, pitch angle control, converter and speed control part [20]. It is possible to directly connect the stator of the DFIG to the power system, while the pulse width modulation inverter is used to link the rotor to the power system. Wind energy is converted into mechanical energy via wind turbines, which can then be converted into electricity. The pitch angle mediation equations of DFIG and the fourth-order model of DFIG in the d-q coordinate axis are given in reference [21, 22].

The PV system is connected to the external power grid and can supply active and reactive power to the power system and is part of the power system. A PV system usually consists of a PV array, a controller, an inverter and a power grid, where the PV array is the key part of the PV system. There are many PV cells in the PV array that are connected in series or in parallel. PV cells consist of PN-type semiconductors and generate current through the photovoltaic effect.

### 2.2 PSS of SGs

A common method of suppressing LFO in power systems is to add PSS to the excitation system of synchronous thermal power generators. As an additional control to the SG's excitation system, when adjusting for voltage variation, PSS can eliminate the negative damping produced by the automatic voltage regulator (AVR) and add positive damping torque to the system. The phase lag between the torque component and rotor speed  $\omega$  can be chosen as the PSS input signal to compensate the excitation system. Otherwise, the power system will become unstable due to increased rotor oscillation [23].

$$\begin{cases} \dot{V}_1 = -(K_w\omega + V_1)/T_w \\ \dot{V}_2 = \left( \left(1 - \frac{T_1}{T_2}\right)(K_w\omega + V_1) - V_2 \right) / T_2 \\ \dot{V}_3 = \left( \left(1 - \frac{T_3}{T_4}\right) \left( V_2 + \left( \frac{T_1}{T_2} (K_w\omega + V_1) \right) \right) - V_3 \right) / T_4 \\ V_S = V_3 + \frac{T_3}{T_4} \left( V_2 + \frac{T_1}{T_2} (K_w\omega + V_1) \right) \end{cases} \quad (1)$$

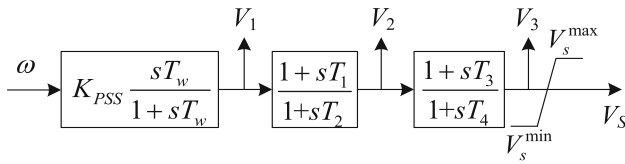


Fig. 2 Structure of PSS

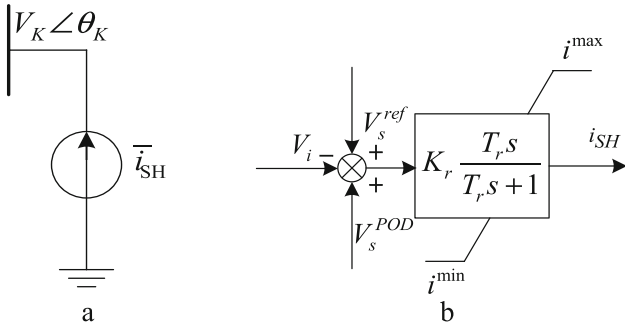


Fig. 3 (a) STATCOM equivalent circuit diagram, (b) STATCOM control block diagram

This paper adopts a PSS consisting of a scour filter with time constant  $T_w$ , a damping gain  $K_{PSS}$  and a lead–lag compensation block with time constants  $T_1, T_2, T_3$  and  $T_4$ , as shown in Fig. 2. AVR’s reference voltage can be modified by the state variable  $V_S$ , which is the output of PSS. Equation (1) provides the value of  $V_S$ .  $V_1, V_2$  and  $V_3$  refer to the output signals of the corresponding blocks.

### 2.3 STATCOM-POD controller

The STATCOM dynamic model is shown in Fig. 3. STATCOM adopts the first-order current injection model described in the literature [24, 25] in this paper. As a parallel FACTS device, STATCOM can provide reactive power support to the power system by adjusting its output current  $i_{SH}$  according to Eq. (2).

(a) STATCOM circuit, (b) STATCOM control block diagram

$$\begin{cases} \dot{i}_{SH} = (K_r(V_{ref} + V_s^{POD} - V_i) - i_{SH})/T_r \\ Q = i_{SH}V_i \end{cases} \quad (2)$$

where regulator’s voltage gain, reference voltage and time constant are represented by  $K_r, V_{ref}$  and  $T_r$ , respectively; the measured voltage and reactive power of STATCOM nodes are denoted by  $V_i$  and  $Q$ , respectively; and  $V_s^{POD}$  is the output voltage of PODC.

The design of PODC includes amplification, DC isolation, phase compensation and current limiting, and Eq. (3) is its transfer function. STATCOM and PODC together constitute a closed-loop control structure. Additional control signals of

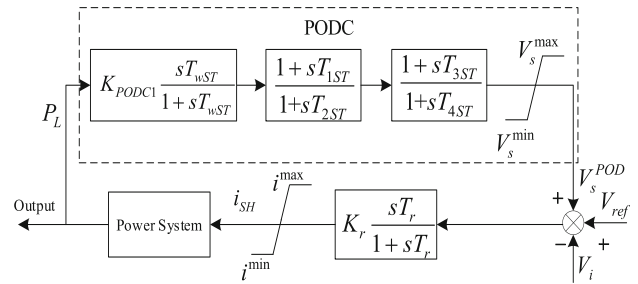


Fig. 4 Control block diagram of STATCOM-PODC

PODC are added to the AC voltage part of STATCOM to maximize the output or absorbed reactive power, effectively increase the system damping and improve the dynamic characteristics of the system.

$$G(s) = K_{POD} \frac{sT_w}{1+sT_w} \frac{1+sT_{POD1}}{1+sT_{POD2}} \frac{1+sT_{POD3}}{1+sT_{POD4}} \quad (3)$$

Figure 4 shows the closed-loop control structure formed by STATCOM and PODC together, where the PODC’s control structure is comparable to the PSSs. A power oscillation damping amount is determined by the value of the stabilizer gain  $K_{POD}$  of PODC. To guarantee that the output of PODC remains zero in steady state, a washout filter with a temporal constant  $T_{bw}$  is utilized. Phase lead characteristics can be provided by using two-phase compensator blocks with time constants  $T_{b1}, T_{b2}, T_{b3}$  and  $T_{b4}$ . Signals for the PODC input are not unique, and local or remote signals may be selected depending on the circumstances, such as the selection of line active and reactive power, current and voltage. In this article, the active power of transmission line  $P_L$  is selected [26].

STATCOM adds the output signal of PODC to its AC voltage control section. To avoid overshoot, there is an anti-windup limiter to limit the adjustment range of  $V_s^{POD}$ . The maximum value of  $V_s^{POD}$  is  $V_s^{max}$ , and the minimum value is  $V_s^{min}$ .

### 2.4 SSSC-POD controller

$$\begin{aligned} \dot{V}_{SC} &= V_{scd} + jV_{scq} \\ &= k'm'V'_{dc} \sin \delta' / \sqrt{2} + jk'm'V'_{dc} \cos \delta' / \sqrt{2} \\ &= k'm'V'_{dc} \angle \delta' / \sqrt{2} \end{aligned} \quad (4)$$

The basic topology of the SSSC is shown in Fig. 5 and consists of a DC capacitor  $C'_{dc}$ , a voltage source inverter (VSI) and a series coupling transformer. The SSSC can operate in capacitive or inductive mode to increase or decrease the transmitted reactive and active power, depending on the polarity of the series injection voltage ( $\dot{V}_{sc}$ ).

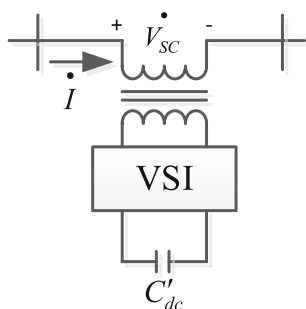


Fig. 5 SSSC structure diagram

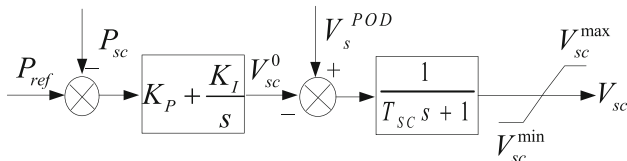


Fig. 6 SSSC control block diagram

Based on the constant voltage control strategy of SSSC in [27], the injection voltage of SSSC in the synchronous coordinate system can be expressed as Eq. (4) [28].

In Eq. (4),  $\delta'$  is the SSSC equivalent voltage amplitude;  $V_{dc}'$  is the SSSC DC capacitor voltage;  $m'$  is the PWM coefficient of the inverter; the transformation ratio of the transformer is  $k'$ ; the  $d$ -axis and  $q$ -axis components of the equivalent voltage at the SSSC node are  $V_{scd}$  and  $V_{scq}$ , respectively; the equivalent voltage of the SSSC node is  $\dot{V}_{sc}$ ; the capacitance is  $C$ ; and  $\dot{I}$  is the current flowing into the power system node.

Suppose the reactance of the transmission line without SSSC is  $X_L$ , and its equivalent compensation capacitive reactance is  $X_C$ , then the compensation degree of SSSC can be expressed as:

$$C_P = X_C / X_L \tag{5}$$

In the formula, the value range of  $C_P$  is [0,1], and the equivalent reactance after adding SSSC is:

$$X'_L = (1 - C_P)X_L \tag{6}$$

Through the analysis of Eq. (5) and (6), it can be known that the constant increase in the  $C_P$  value will lead to the continuous decrease, the equivalent electrical distance of the line will be shortened, and the power transmission limit of the system will be increased, and the system stability will be improved.

The SSSC control block diagram used in this paper is given in Fig. 6. In the figure, the equivalent voltage value of SSSC is  $V_{sc}$ ;  $V_{sc}^{max}$  and  $V_{sc}^{min}$  are the upper and lower limits of  $V_{sc}$ , respectively; the time constant of the SSSC voltage

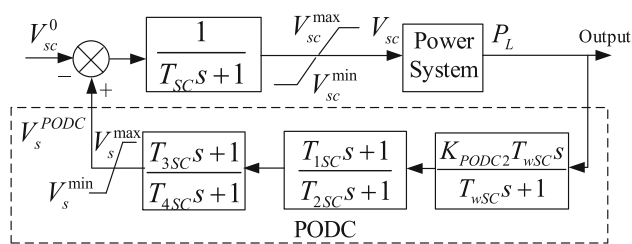


Fig. 7 SSSC-PODC control block diagram

regulator is TSC; the output voltage of the PODC is  $V_s^{PODC}$ ; the initial value of the SSSC compensation voltage is  $V_{sc}^0$ ; the proportional and integral coefficients of the PI control link are  $K_P$  and  $K_I$ , respectively; the power value at the SSSC installation is  $P_{sc}$ ; and the power reference value is  $P_{ref}$ .

The basic principle of PODC control has been introduced in Sect. 2.3. The design of SSSC-PODC control block diagram is shown in Fig. 7. SSSC and PODC together form a closed-loop control structure, and the phase compensation link is used to compensate the phase lag between the PODC input signal  $y$  and the bus voltage at the SSSC installation; the limiting link is used to limit the amplitude of the PODC control link regulation signal. The output voltage of the PODC controller is used as an additional control signal, which is connected to the voltage regulator of the SSSC, so that the equivalent voltage of the SSSC is regulated to provide additional damping control and further improve the ability of the SSSC to improve the damping characteristics.

### 3 Parameter optimization problem description

This section discusses how to solve the coordination problem between PSSs, STATCOM-PODC and SSSC-PODC controllers convert to a problem of finding the objective function's extreme value. It is possible to suppress the LFO of the system while maintaining voltage stability by coordinating the different controllers.

#### 3.1 For small-signal stability

A differential algebraic equation can be used to represent the WPTB transmission system's state space, as shown in Eq. (7).

$$\begin{cases} \dot{x} = f(x, y) \\ 0 = g(x, y) \end{cases} \tag{7}$$

where  $x$  and  $y$ , respectively, represent the state variables' and algebraic variables' vectors.



Based on linearization theory and Lyapunov theory, the best technique for examining the stability of small signals in power systems is eigenvalue analysis. The linearized model of the system can be obtained by Taylor series expansion at the stable operating point  $(x_s, y_s)$ , expressed in Eq. (8).

$$\begin{bmatrix} \Delta \dot{x} \\ 0 \end{bmatrix} = \begin{bmatrix} \nabla_x f & \nabla_y f \\ \nabla_x g & \nabla_y g \end{bmatrix} \begin{bmatrix} \Delta x \\ \Delta y \end{bmatrix} = \begin{bmatrix} A_1 & B_1 \\ C_1 & D_1 \end{bmatrix} \begin{bmatrix} \Delta x \\ \Delta y \end{bmatrix} \quad (8)$$

where  $\nabla_x f$  is the gradient of the function  $f(x, y)$ , and  $\nabla_x f = \partial f(x, y)/\partial x$ , and the other remaining similar symbols have similar definitions. By considering  $\nabla_x g$  is non-singular, then (8) can be written as:

$$\Delta \dot{x} = [A_1 - B_1(C_1)^{-1}D_1]\Delta x = A\Delta x \quad (9)$$

where  $A$  is the state matrix, suppose the complex eigenvalues of  $A$  are  $\lambda = \alpha \pm j\beta$ , then the oscillation frequency is  $f = \beta/2\pi$ . Equation (10) gives the damping ratio of the system:

$$\xi(\%) = \frac{-\alpha}{\sqrt{\alpha^2 + \beta^2}} \times 100\% \quad (10)$$

The relationship between system modes and state variables can be expressed by participating factors. As the value increases, the mode contribution to dynamic response will increase as well. The formula for calculating it is as follows:

$$p_{ij} = w_{ij}v_{ji}/(w_i^T v_i) \quad (11)$$

where  $w$  and  $v$  are  $A$ 's left eigenvector and right eigenvector, respectively, and  $p_{ij}$  is the  $i$ th state variable's participation factor to the  $j$ th eigenvalue. For any eigenvalue  $\lambda_i$ , the right eigenvector of  $\lambda_i$  is the  $n$ -column vector meeting the condition  $Av_i = \lambda_i v_i (i = 1, 2, \dots, n)$ ; the  $n$ -row vector  $w_i$  satisfying  $w_i^T A = w_i^T \lambda_i (i = 1, 2, \dots, n)$  is called the left eigenvector of  $\lambda_i$ . And participation factor determines the dominant machines of LFO modes.

To suppress power oscillations, the objective function is designed for the parameter coordination problem of PSS, SSSC-PODC and STATCOM-PODC. Considering the damping ratio of each LFO mode, the maximum damping ratio is 1. With the iteration of the algorithm, the damping ratio of each oscillation mode of the system is closer and closer to 1, thus increasing the damping ratio. Therefore, the ultimate objective of this optimization is to maximize the damping ratio, and power angle stability can be defined as follows:

$$\min J_1 = \min \sum_{i=1}^q (1 - \xi_i) \quad (12)$$

where  $\xi_i$  is the damping ratio of the  $i$ th LFO mode of the system.

### 3.2 For transient voltage stability

When considering the voltage stability of the transmission system, taking into account the amplitude of voltage oscillation in the transient process of the transmission system and the time required to restore stability, the objective function is defined as:

$$\min J_2 = w_1 \int_{t_0}^{t_s} \sum_{k=1}^n [V_k(t) - V_k(0)]^2 dt - w_2 \sum_{k=1}^n V_{k \min} \quad (13)$$

where  $t_0$  and  $t_s$  represent the fault's and the simulation's respective end times;  $V_k(t)$  is the  $k$ th node's voltage amplitude at time  $t$ ;  $V_k(0)$  stands for voltage prior to a fault;  $V_{k \min}$  is the  $k$ th node's minimum voltage; and  $w_1$  and  $w_2$  are the weighting coefficients. In this paper, the  $w_1$  and  $w_2$  as  $1/[n \times (t_d - t_0)]$  and 1. The stability of the system's transient voltage increases with decreasing the objective function.

In order to optimize STATCOM-PODCs and PSSs, small-signal stability and voltage stability must be considered simultaneously, and a comprehensive consideration of  $J_1$  and  $J_2$  is required in the establishment of the optimization objective function. The objective function is as follows:

$$J = W_1 J_1 + W_2 J_2 \quad (14)$$

where  $W_1$  and  $W_2$  are the weight coefficients of  $J_1$  and  $J_2$ , respectively. The values of  $W_1$  and  $W_2$  can be determined according to the actual system's structure and how serious stability issues are. In this paper, the value of  $W_1$  is 1, and the value of  $W_2$  is 0.5.

According to the aforementioned theory, the STATCOM-PODC, SSSC-PODC and PSS parameter optimization issue may be expressed as:

Minimize  $J$ .

According to Sect. 2.2, the constraints of PSS controllers can be defined as:

$$B_{\min} \leq B \leq B_{\max} \quad (15)$$

According to Sect. 2.3, the STACOM-PODC constraints can be defined as:

$$C_{\min} \leq C \leq C_{\max} \quad (16)$$

According to Sect. 2.4, the SSSC-PODC constraints can be defined as:

$$D_{\min} \leq D \leq D_{\max} \quad (17)$$

where  $B$ ,  $C$  and  $D$  are the parameters of the PSS, STATCOM-PODC and SSSC-PODC, respectively, which are defined as  $B = [K_{PSS}, T_1, T_3]$ ,  $C = [K_{PODC1}, K_r, T_r, T_{1ST}, T_{2ST}, T_{3ST}, T_{4ST}]$  and  $D = [C_P, K_{PODC2}, T_{1SC}, T_{2SC}, T_{3SC}, T_{4SC}]$ .  $B_{\min}$  and  $B_{\max}$  are the lower and upper limits of the parameters of PSS controllers;  $C_{\min}$  and  $C_{\max}$  restrict the minimum and maximum limits of the parameters of STATCOM-PODC controller.  $D_{\min}$  and  $D_{\max}$  are the lower and upper limits of the parameters of SSSC-PODC controller. The controller's parameters are optimized in order to minimize the objective function. Convergence of an algorithm can be sped up by using a reasonable parameter range. Within this article, the gain constant parameters range from 1 to 50, the time constant limits range from 0.01 to 2, and the CP value range is given in Sect. 2.4.

## 4 Solution methodology

### 4.1 Adaptive droop coefficient control

The PSO algorithm is based on the regularity of bird predation which can quickly find the optimal solution of the problem. In  $d$ -dimensional space, think of each particle as having no mass or volume, moving across the search space at a certain speed, adjusting this velocity dynamically based on a review of both individual and group flying experience, and updating the individual's location as necessary. PSO performs a global search under individual adaptive conditions to generate particles with random velocity and position, and then initializes the population. Following the local best position of each particle as well as the global best position, PSO is continually updating the velocity and position of each particle during the search process, and it can be expressed as:

$$\begin{cases} V_{i,d}^{k+1} = \omega V_{i,d}^k + c_1 r_1 (P_{i,d}^k - X_{i,d}^k) + c_2 r_2 (P_{gd}^k - X_{i,d}^k) \\ X_{i,d}^{k+1} = X_{i,d}^k + V_{i,d}^{k+1} \end{cases} \quad (18)$$

where  $V_{i,d}^k$  and  $X_{i,d}^k$  symbolize the speed and location of the  $d$ th dimension of particle  $i$  in the  $k$ th iteration, respectively;  $r_1$  and  $r_2$  are used to increase the randomness of the particles, generally taking random constants between 0 and 1;  $P_{i,d}^k$  is the current local best, which indicates the optimal position of particle  $i$  in the  $d$ th dimension in the  $k$ th iteration;  $P_{gd}^k$  is the current global best, which symbolizes the optimal position of the  $d$ th dimension of the population in the  $k$ th iteration;  $c_1$  and  $c_2$  are impact factors, which demonstrate the effect of  $P_{id}$  and  $P_{gd}$  on the speed of the recent particle; and  $\omega$  is the inertia weight, and its purpose is to preserve the particles' original properties and govern their exploring abilities. The particles may be made to have a balanced search capability

by selecting a suitable value of  $\omega$ , which reduces the average number of iterations needed to obtain an optimal solution. The value of  $\omega$  is established in this paper by (19).

$$\omega = \begin{cases} \omega_{\min} - \frac{(\omega_{\max} - \omega_{\min}) * (f - f_{\min})}{f_{avg} - f_{\min}}, & f \leq f_{avg} \\ \omega_{\max}, & f > f_{avg} \end{cases} \quad (19)$$

where the lowest and upper limits of inertia weight are  $\omega_{\max}$  and  $\omega_{\min}$ , respectively, and  $f$  is the fitness value of the current particle. The average and minimum fitness values for the total population of particles are represented by  $f_{avg}$  and  $f_{min}$ , respectively.

According to (19), in the neighborhood of the current optimal solution, particles with higher individual fitness will conduct local detailed searches, whereas particles with lower individual fitness will search at a wider step size in order to locate a better solution, ensuring that the entire group of solutions remains diverse and converges well.

However, with increasing PSO iterations, the diversity of particle swarms is easily destroyed and falls into local optimum. On the basis of PSO, this paper proposes using GA to perform crossovers and mutations on the population, which is helpful for enhancing particles' capacity for global optimization and causes the algorithm to depart from the local optimum point.

### 4.2 Solution procedure

The PSO-GA optimization algorithm combines GA's randomness with PSO's advantages to enhance global optimization capabilities. The parameters of each controller that has a great influence on the stability of the power system are extracted as the parameters to be optimized in the PSO-GA algorithm. The initial value of the controller parameters represents the initial position of the particle, and the particle optimization direction and speed are assigned according to the corresponding rules, and are limited to a certain range, which represents the upper and lower limits of the controller parameters. After the completion of each iteration, the particle with the best optimization effect will be selected as the optimal solution according to the objective function. In this way, the most suitable particle position is found through layers of iteration, that is, the coordinated controller parameter value. Figure 8 shows the proposed algorithm process for optimizing the STATCOM-PODC, SSSC-PODC and PSS parameters.

The optimization process shown in Fig. 8 is described as follows:

- (1) Initialize the value of optimized parameters  $K_{PSS}$ ,  $K_r$ ,  $K_{PODC1}$ ,  $K_{PODC2}$ ,  $T_1$ ,  $T_3$ ,  $T_r$ ,  $T_{1ST}$  to  $T_{4ST}$ ,  $T_{1SC}$  to  $T_{4SC}$ , of PSSs, STATCOM-PODC and SSSC-PODC by

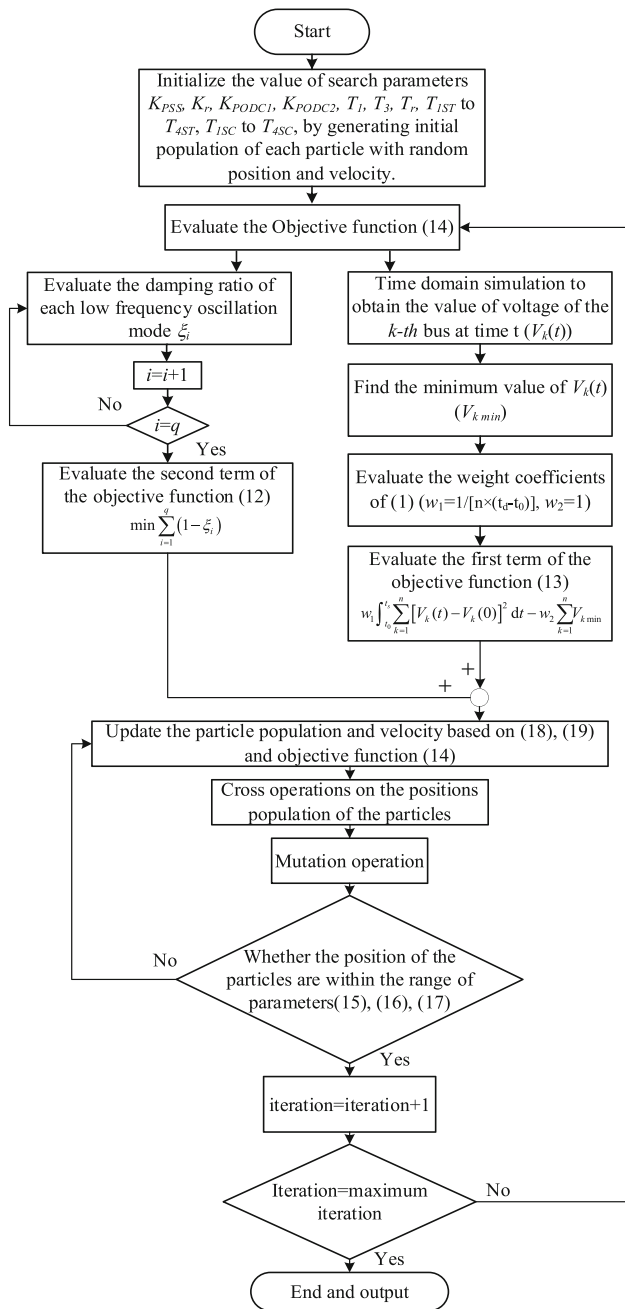


Fig. 8 Flowchart of parameter optimization based on PSO-GA

creating initial population of each particle with random speed and location. Here, the final position of each particle represents a solution to this parameter.

(2) Assess the goal function (14). In the first part of the objective function, eigenvalue analysis is used to calculate the damping ratio of each LFO mode. The second part objective function using time-domain simulation.

- (a) For the first part of the goal function.
  - (i) Assess  $\xi_i$  each LFO mode’s damping ratio.
  - (ii)  $i = i + 1$

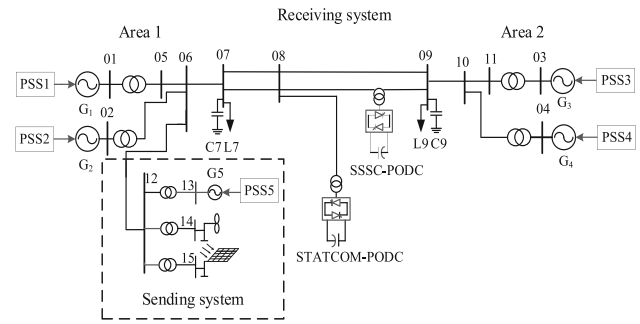


Fig. 9 Modified 4-machine 2-area system

- (iii) Evaluate (12). Suppose the power system has  $q$  LFO modes. If  $i = q$ , go to 4), if  $i < q$ , go to a).
- (b) For the second part of the goal function.
  - (i) Time-domain simulation to obtain the value of voltage of the  $k$ th bus at time  $t$ .
  - (ii) Find the minimum value of  $V_k(t)$  ( $V_{k\min}$ ).
  - (iii) Assess the weight coefficients of (13) ( $w_1 = 1/[n \times (t_d - t_0)]$ ,  $w_2 = 1$ ).
  - (iv) Evaluate (13).
- (3) Update the location population and velocity population of the particles based on (18), (19) and goal function (14).
- (4) Cross operations on the location of the particles.
- (5) Mutation operation.
- (6) Verify that the particle locations are fall inside the parameters’ range, and the out-of-range particle is fixed at the boundary.
- (7) Iteration = iteration + 1.

The procedure stops when it achieves the maximum number of iterations. Otherwise, go to (2).

## 5 System studies

### 5.1 Modified 4-machine 2-area system

As shown in Fig. 9, based on the MATLAB/Simulink simulation environment, an improved IEEE 4-machine 2-area system simulation model has been developed. WPTB sending end system is connected to the Bus 06, and the output of the three power sources is, respectively, 30, 40 and 300 MW. In order to analyze conveniently, this paper replaces lumped models of wind farms and PV stations with wind turbines and PV stand-alone models. There are 4 strongly coupled large SGs at the receiving end of the system. Turbine governor (TG) is unified for SGs and PSS is installed for AVR, and the base capacity of SGs are set to 100 MVA, and the



basic transmission power of the tie line is 400 MW. STATCOM adopts the first-order current injection model, adjusts the output current  $i_{SH}$  according to Eq. (2). The SSSC adopts the constant voltage control strategy, and its injection voltage is Eq. (3). With the help of the residue index of the open-loop system [29], consider connecting SSSC-PODC between Bus 08 and Bus 09, and connecting STATCOM-PODC in Bus 08.

Based on the example system shown in Fig. 9, the following sections systematically study the coordinated optimization effect of PSO-GA on multi-controller parameters and verify the effect of the optimized controller on the system. The STATCOM-PODC is connected in parallel to Bus 8 and the SSSC-PODC is connected in series to the line between Bus 8 and Bus 9. The three cases listed below are comparison tests to verify the performance of the controller and the effectiveness of the optimization algorithm:

*Case 1* Only access PSS.

*Case 2* Access PSS, STATCOM-PODC and SSSC-PODC without optimizing their parameters.

*Case 3* Access PSS, STATCOM-PODC and SSSC-PODC, and coordinate and optimize parameters.

The controller parameters before optimization in case 1 can be found in reference [30]. The paper makes some modifications based on the actual simulation model situation. Presented in Appendix are the parameters for Case 1 without optimization and Case 2 with optimization.

### 5.2 Analysis of eigenvalues and time-domain simulation results

Based on the three operating conditions of the system, Table 1 presents characteristic values associated with the LFO modes. Equation (9) calculates the eigenvalues of A, and as WPTB sources is connected to the power system, two LFO modes will be added to the system, aggravate the oscillation of the system compared to the three modes of the traditional 4-machine 2-area system. A look at the DMs in Table 1 illustrates that Modes 1 and Modes 2 represent the local oscillations of Areas 1 and 2, respectively; Modes 3 and Modes 4 represent the inter-area oscillations between sending end and receiving end systems. Mode 5 is the inter-area oscillation mode among all units.

In Case 2, the damping ratios of Mode 2, Mode 3 and Mode 5 increased to different degrees, increasing by 0.19, 1.08 and 10.36%, respectively. However, the damping ratio of Mode 1 and Mode 4 decreased by 0.36 and 3.71%, respectively, especially for oscillation Mode 4 (the part with black font), the damping ratio decreased to 2.25%, and its eigenvalues were closer to the left half of the complex plane. The system has a great chance of destabilizing in case of disturbance. In Case 3, the overall damping ratio of the system is

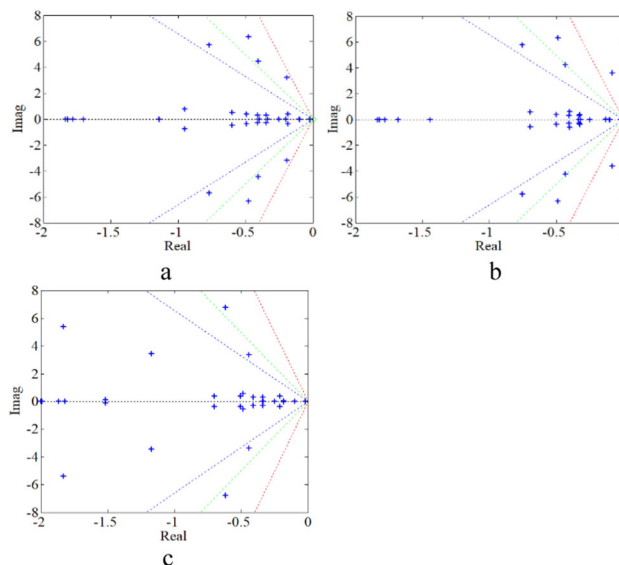


**Fig. 10** Characteristic root distribution diagram of the system under three working conditions: (a) Case 1 eigenvalue distribution, (b) Case 2 eigenvalue distribution, (c) Case 3 eigenvalue distribution

significantly improved. The total damping of the LFO modes is 55.55% higher than that of Case 1 and 47.99% higher than that of Case 2. The eigenvalue analysis results show that simply adding controllers without considering the coordination of parameters does not significantly improve the stability of the power system, and may even worsen the stability of the system. The controller optimized by the algorithm can significantly improve the damping ratio of the system and suppress the LFO of the system.

After PSO-GA optimization, the improvement effect of inter-area oscillation Mode 4 (the part with black font) is the most significant, and the damping is increased by 29.83% compared with that before optimization. The controller using algorithm optimization parameters shifts the eigenvalues originally closer to the right half of the complex plane to the left, which significantly improves system stability. Therefore, using the PSO-GA algorithm to optimize the parameters of PSS, STATCOM-PODC and SSSC-PODC can improve the damping ratio of the system and suppress the LFO.

Figure 10 shows the distribution of all eigenvalues of the system on the complex plane under three different situations. And the horizontal axis is the real part of the eigenvalue, the vertical axis is the imaginary part of the eigenvalue. The blue, green and red dashed lines represent equal damping ratio lines with damping ratios of 5, 10 and 15%, respectively. As shown in Fig. 10, the access to SSSC-PODC and STATCOM-PODC causes a significant rightward shift in the eigenvalues of mode 4 in the complex plane compared to Case 1, and the eigenvalues that were originally inside the red line are shifted to the right outside the red line. Compared with Case 3, Case 2 has two pairs of eigenvalues with a damping ratio around

**Table 1** LFO modes of the system under three working conditions

Mode	Case	$\lambda$	$\xi/1\%$	$f/\text{Hz}$	DMs
Mode 1	1	$-0.7685 \pm j5.7070$	13.33	0.9082	$G_1 G_2$
	2	$-0.7549 \pm j5.7734$	12.97	0.91889	
	3	$-1.8287 \pm j5.3845$	32.16	0.8570	
Mode 2	1	$-0.4758 \pm j6.3467$	7.48	1.0101	$G_3 G_4$
	2	$-0.4860 \pm j6.3232$	7.67	1.0064	
	3	$-0.6182 \pm j6.7877$	9.07	1.0803	
Mode 3	1	$-1.8287 \pm j5.3845$	9.04	0.8570	$G_1 G_2 G_5$
	2	$-0.4294 \pm j4.2248$	10.12	0.6724	
	3	$-0.4420 \pm j3.3633$	13.03	0.5353	
Mode 4	1	$-0.1908 \pm j3.1933$	<b>5.96</b>	0.5082	$G_3\text{-}G_5$
	2	$-0.0811 \pm j3.6091$	<b>2.25</b>	0.5744	
	3	$-1.1718 \pm j3.4595$	<b>32.08</b>	0.5506	
Mode 5	1	$-0.1844 \pm j0.3841$	43.28	0.0611	$G_1\text{-}G_5$ DFIG PV
	2	$-0.3996 \pm j0.6287$	53.64	0.1000	
	3	$-0.2091 \pm j0.3791$	48.30	0.0603	

By simply adding controllers without considering parameter coordination, the system is at risk of instability in some modes

5%, and its damping level is smaller, which proves that the improvement effect of the uncoordinated controller on the system is not ideal, and may even deteriorate the system stability. In Case 3, the PSO-GA-based optimization shifts the real part of the system eigenvalues toward the left part of the complex plane, and most of the system eigenvalues in Case 3 are distributed within the 10% equal damping ratio line, with only two pairs of eigenvalues located around 10%, which undoubtedly improves the small disturbance stability of the system.

Figure 11 shows the fault response curves when a three-phase short-circuit fault occurs under different Cases, assuming that the three-phase short-circuit fault occurs on the tie line from Bus 07 to Bus 09, with fault occurrence time  $t = 1$  s, end time  $t = 1.1$  s and simulation time set to 30 s. Time-domain simulation results show that in Case 2, the power angle curve of generator G1 was improved to some extent, but the improvement was not significant, and the system stabilized around 27 s. However, in Case 3, the maximum power angle oscillation amplitude of the generator is reduced by nearly 0.3 rad, and the oscillation is suppressed quickly, and the system stabilizes around the 15th s. The stabilization time is advanced by 12 s, which greatly reduces the oscillation time. By analyzing the voltage curves of Bus 12 and Bus 01, the system voltage oscillation is somewhat attenuated in Case 2, but its improvement effect is small. This shows that after optimization by PSO-GA algorithm, multiple controllers give full play their respective roles, significantly suppress the voltage oscillation of the system and improve the stability of the system.

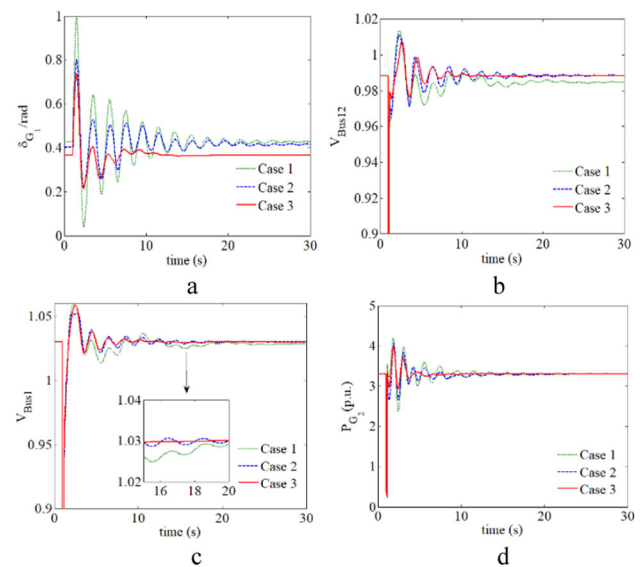


**Fig. 11** Three-phase short-circuit response curve under three cases: (a) Generator G1 relative power angle curve, (b) Bus 12 voltage curve, (c) Bus 01 voltage curve, (d) Generator G2 active power output curve

### 5.3 System simulation when the output of wind and PV unit was changed.

To analyze the effect of PSS, STATCOM-PODC and SSSC-PODC on system improvement, this section investigates the effect of multi-controller on power system stability after parameter optimization using PSO-GA, based on the coordinated optimization parameters, while varying the wind turbine and PV unit outputs. In this section, the wind and

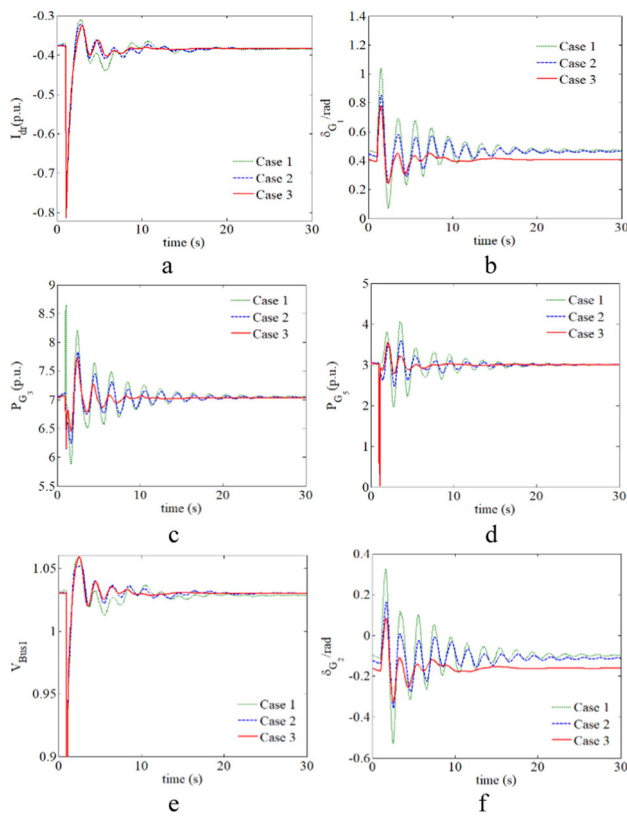


**Fig. 12** Three-phase short-circuit response curve of the system when the output of DFIG and PV changes (a) d-axis rotor current  $I_{dr}$  curve of DFIG, (b) Generator G1 relative power angle curve, (c) Generator G3 active power output curve, (d) Generator G5 active power output curve, (e) Bus 1 voltage curve, (f) Generator G2 power angle curve

PV output is increased by 30%, and the three cases' conditions of the system in this subsection are the same as in Sect. 5.1.

Table 2 gives the eigenvalues of the system under the three cases. From the data in the table, it can be seen that compared to Case 1 in Table 2, the damping ratios of Modes 1, 3, 4 and 5 are reduced to different degrees, by 0.03, 0.02, 0.01 and 7.12%, respectively, which shows that when the output of new energy units increases, it may cause adverse effects on the system. In Case 2 of Table 2, the total damping ratio of the system is slightly improved to 1.7%, but the damping ratio of interregional oscillation Mode 4 is still closer to the right half of the complex plane, and it is obvious that the uncoordinated controller cannot exert the best control effect. The eigenvalue analysis results show that after optimization by PSO-GA algorithm, the improvement effect of the inter-area oscillation mode 4 is the most significant, and the damping is increased by 29.39% compared with that before the optimization.

If a three-phase short-circuit fault occurs in the system as in the previous section, Fig. 12 shows the response curve of the system. Comparing the relative power angle curves of

generator G1 in Figs. 10 and 11, the amplitude of the system work angle curve is also greater when both wind and PV power output increases, with the amplitude of oscillation increasing by about 0.03 rad. And in Case 2 of Fig. 11, with the addition of multiple controllers, the power angle curves of G1 and G3, the d-axis rotor current of DFIG and the active output curve of G5 are improved to some extent despite the increase in the output of the new energy unit under the synergistic control of PSS, STATCOM-PODC and SSSC-PODC. Time-domain simulation results show that after optimization by PSO-GA algorithm, it is obvious that the amplitude of system power angle oscillation and active power oscillation are further reduced at the time of fault occurrence, and the system voltage oscillation is also significantly suppressed, and the time required to restore the system stability is also reduced, which proves the effectiveness of the proposed parameter optimization method.

### 5.4 The optimization effect of the algorithm when changing the transmission power of the tie line

Changes in generator output as well as load power will cause changes in the transmission power of the tie line. In this subsection, the power transmitted by the tie line is changed by adjusting the power output of the thermal generating units in area 1. The power transmission direction of the tie line is from area 1 to area 2, and the improvement effect of the optimized multi-controller on the damping ratios of the system oscillation modes and its fault response curves are investigated.

The eigenvalues and damping ratio of the system when the transmission power of the tie line decreases by 50 MW and increases by 100 MW are shown in Table 2. The meanings of the three working conditions are the same as those in Sect. 5.1. In Case 1, as the power of the tie line increases from 350 to 500 MW, the damping ratios of oscillation Modes 1, 3 and 4 decrease by 2.81, 2 and 0.23%, respectively, and the damping ratios of Modes 2 and 5 increase by 0.44 and 1.57%, respectively, and the total damping ratio of the system decreases by 3.03%, which shows that the increase in the tie line transmission power has a negative impact on the system stability. Comparing Case 1 and Case 3 with the same transmission power of the tie line, the damping ratio of the system increases significantly in the case of Case 3. The total damping ratio increases by 51.945% for 350 MW transmission power of the tie line and by 60.19% for 500 MW transmission power of the tie line. This fully illustrates that the multi-controller optimized by the PSO-GA algorithm has a significant effect on the improvement of the damping ratio of the system, and its parameters have a certain degree of robustness to adapt to the variation of the transmission power of the tie line.

**Table 2** LFO modes of the system in different cases after the output of new energy units increases

Mode	Case	$\lambda$	$\xi/\%$	$f/\text{Hz}$	DMs
Mode 1	1	$-0.7676 \pm j5.7062$	13.3	0.91	$G_1 G_2$
	2	$-0.7533 \pm j5.7681$	12.95	0.92	
	3	$-1.8202 \pm j5.3904$	31.99	0.86	
Mode 2	1	$-0.4789 \pm j6.3485$	7.52	1.01	$G_3 G_4$
	2	$-0.4867 \pm j6.3303$	7.67	1.01	
	3	$-0.6195 \pm j6.7931$	9.08	1.08	
Mode 3	1	$-0.4023 \pm j4.4430$	9.02	0.71	$G_1 G_2 G_5$
	2	$-0.4203 \pm j4.2330$	9.88	0.67	
	3	$-0.4495 \pm j 3.349$	13.31	0.53	
Mode 4	1	$-0.1905 \pm j3.1936$	5.95	0.51	$G_3\text{-}G_5$
	2	$-0.0906 \pm j3.5128$	2.6	0.56	
	3	$-1.1676 \pm j3.4599$	31.99	0.55	
Mode 5	1	$-0.1927 \pm j0.4968$	36.16	0.08	$G_1\text{-}G_5$ DFIG PV
	2	$-0.3446 \pm j0.7767$	40.55	0.12	
	3	$-0.2395 \pm 0.5157$	42.11	0.08	

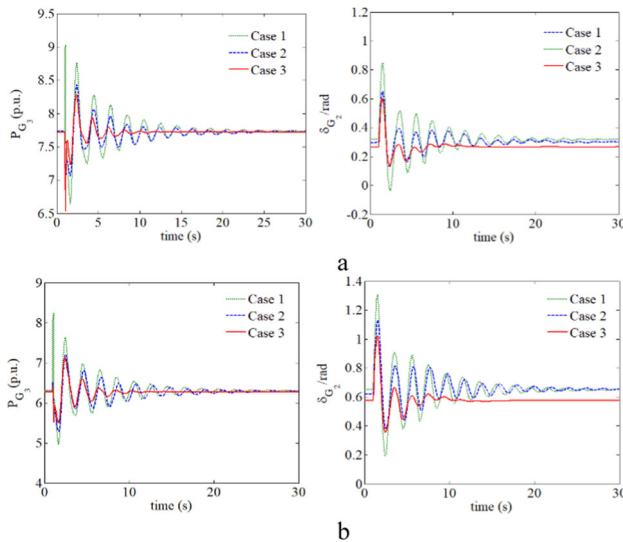


**Fig. 13** Three-phase short-circuit response curves of the system when the power of the tie line is different. (a) The transmission power of the tie line is 350 MW. (b) The transmission power of the tie line is 500 MW

The system is simulated in the time domain with a simulation time of 30 s. Assuming the same fault occurrence as in Sect. 5.2, Fig. 13 shows the three-phase short-circuit response curve of the system at different contact line powers. It can be seen from the figure that when the system tie line transmission power increases, if a three-phase short-circuit fault occurs, the system will generate a greater degree of oscillation, which confirms the results of the eigenvalue analysis, the tie line transmission power will be too large to cause adverse effects on the system. Comparing Fig. 12a–d, in Case 1 and Case 2, the system will be stable at about  $t = 25$  s, and

in Case 3, the system will be stable at about  $t = 15$  s, and the stabilization time will be earlier for about 10 s. When a three-phase short-circuit fault comes, the response curves of Case 1 and Case 2 oscillate considerably. From the values of the vertical axis, the amplitude of oscillation is significantly reduced by the algorithm-optimized controller, which shows that even if the tie line transmission power changes, the PSS, STATCOM-PODC and SSSC-PODC optimized based on the PSO-GA algorithm can still achieve coordinated cooperation and jointly enhance the stability of the system.

## 6 Conclusions and prospects

In this paper, a parameter coordination optimization method based on PSO-GA algorithm is proposed for STATCOM-PODC, SSSC-PODC and PSS parameters. The IEEE 4-machine 2-area system is used as a case study and shown that the optimization method is effective by analyzing the eigenvalues and simulation results. The following is a summary of the main conclusions:

- (1) To enhance the improvement effect of STATCOM and SSSC on system stability, the SSSC-PODC and STATCOM-PODC controllers were designed using the active power signal of the tie line as the PODC input signal.
- (2) Construct an objective function based on eigenvalues and damping ratios of the LFO modes, and consider system voltage stability comprehensively. The parameter optimization problem is transformed into the problem of taking the extreme value of the objective function.

The PSO-GA algorithm is used to achieve coordinated optimization of the parameters to maximize the damping ratio of the system in LFO modes and significantly suppress the system voltage oscillation due to faults.

- (3) Finally, the optimization results were verified in the IEEE 4-machine 2-area system using eigenvalue analysis and dynamic time-domain simulation method. The results show that the synergistic optimization of STATCOM-PODC, SSSC-PODC and PSS can significantly improve the overall damping level of the system, enhance the system anti-interference capability and effectively improve the stability of the system. This also proves that the proposed parameter optimization method can solve the parameter coordination optimization problem of PSS and multi-type FACTS devices.

Based on the current research results and methods, the future research direction is prospected as follows:

- (1) In the power system modeling, different types of fan models will be considered, and the power system with multiple fans is optimized by different types of PSS.
- (2) Innovation will be carried out in the design of the objective function, which effectively combined eigenvalue analysis, time-domain simulation, economic problems, the proportion of output between new energy and the proportion of output between new energy and conventional energy, etc., to ensure that the optimized power system can meet the needs of all aspects
- (3) Considering the influence of wind power output fluctuation on the stability of the power system, in order to better consider the uncertainty and ensure the stable and efficient operation of the power system under multiple operation modes, it is planned to adopt the stability analysis of small interference probability to solve the problem of LFO of the power system caused by the uncertainty of wind power output.

**Author's contribution** PH and ZP developed the idea of the study, analyzed the data and wrote the paper. JF completed mathematical modeling. YT and MW designed and polished the figures.

**Funding** This work is supported by the National Natural Science Foundation of China (NSFC) (No. 52377125) and the Scientific and Technological Research Foundation of Henan Province (No. 222102320198). The authors have no relevant financial or non-financial interests to disclose. All authors certify that they have no affiliations with or involvement in any organization or entity with any financial interest or non-financial interest in the subject matter or materials discussed in this manuscript. The authors have no financial or proprietary interests in any material discussed in this article. Preprint statement: This manuscript has been preprinted [<https://doi.org/10.22541/au.166682234.41889369/v1>].

**Data availability** The datasets used or analyzed during the current study are available from the corresponding author on reasonable request.

## Declarations

**Conflict of interest** The authors declare that they have no known competing financial interests or personal relationships that could have appeared to influence the work reported in this paper.

## Appendix

STATCOM-PODC, SSSC-PODC and PSS parameters.

See Tables 3 and 4.



**Table 3** Non-optimization parameters in IEEE 4-machine 2-area system

PSSs	PSS number	$K_{PSS}$	$T_w$	$T_1$	$T_2$	$T_3$	$T_4$	
	1	10	0.5	0.1	0.05	0.01	0.005	
	2	10	0.5	0.1	0.05	0.01	0.005	
	3	10	0.5	0.1	0.05	0.01	0.005	
	4	10	0.5	0.1	0.05	0.01	0.005	
	5	10	0.5	0.1	0.05	0.01	0.005	
STATCOM-PODC	$K_r$	$T_r$	$K_{PODC1}$	$T_{wST}$	$T_{1ST}$	$T_{2ST}$	$T_{3ST}$	$T_{4ST}$
	20	0.1	-0.1	5	0.4	0.2	0.4	0.2
SSSC-PODC	$C_P$	$T_{SC}$	$K_{PODC2}$	$T_{wSC}$	$T_{1SC}$	$T_{2SC}$	$T_{3SC}$	$T_{4SC}$
	30	0.1	-0.1	5	0.4	0.2	0.4	0.2

**Table 4** Optimized parameters in IEEE 4-machine 2-area system

PSSs	PSS number	$K_{PSS}$	$T_w$	$T_1$	$T_2$	$T_3$	$T_4$	
	1	18.3813	0.5	0.4754	0.05	0.3361	0.005	
	2	9.8582	0.5	0.5970	0.05	0.6186	0.005	
	3	41.5714	0.5	0.1810	0.05	0.0460	0.005	
	4	31.6670	0.5	0.7139	0.05	0.5000	0.005	
	5	35.7432	0.5	0.3559	0.05	0.0451	0.005	
STATCOM-PODC	$K_r$	$T_r$	$K_{PODC1}$	$T_{wST}$	$T_{1ST}$	$T_{2ST}$	$T_{3ST}$	$T_{4ST}$
	12.8103	0.4537	0.5668	5	0.7503	1	0.1149	0.3810
SSSC-PODC	$C_P$	$T_{SC}$	$K_{PODC2}$	$T_{wSC}$	$T_{1SC}$	$T_{2SC}$	$T_{3SC}$	$T_{4SC}$
	42.6407	0.1	-0.0323	5	0.3354	0.5502	0.5422	0.3096

## References

- He LC, Lu ZG, Geng LJ, Zhang JF, Li XP, Guo XQ (2020) Environmental economic dispatch of integrated regional energy system considering integrated demand response. *Int J Electr Power Energy Syst* 116:105525. <https://doi.org/10.1016/j.ijepes.2019.105525>
- Khasanov M, Kamel S, Rahmann C, Hasanien HM, Al-Durra A (2021) Optimal distributed generation and battery energy storage units integration in distribution systems considering power generation uncertainty. *IET Gener Transm Distrib* 15(24):3400–3422. <https://doi.org/10.1049/gtd2.12230>
- Liu SY, Lin ZZ, Jiang YC, Zhang TH, Yang L, Tan WT, Lu F (2022) Modelling and discussion on emission reduction transformation path of China's electric power industry under "double carbon" goal. *Heliyon* 8(9):e10497. <https://doi.org/10.1016/j.heliyon.2022.e10497>
- Pei W, Zhang X, Deng W, Tang CH, Yao LZ (2022) Review of operational control strategy for DC microgrids with electric-hydrogen hybrid storage systems. *CSEE J Power Energy Syst* 8(2):329–346
- He P, Wu XX, Li CS, Zheng MM, Li Z (2020) Improvement of damping characteristics and index evaluation of a wind-PV-thermal-bundled power transmission system by combining PSS and SSSC. *Archiv Electr Eng*. <https://doi.org/10.24425/ae.2020.133927>
- Dong J, Dou ZH, Si SQ, Wang ZC, Liu LX (2022) Optimization of capacity configuration of wind-solar-diesel-storage using improved sparrow search algorithm. *J Electr Eng Technol* 17(1):1–14. <https://doi.org/10.1007/s42835-021-00840-3>
- Ranamuka D, Muttaqi KM, Sutanto D (2019) Flexible AC power flow control in distribution systems by coordinated control of distributed solar-PV and battery energy storage units. *IEEE Trans Sustain Energy* 11(4):2054–2062. <https://doi.org/10.1109/TSSTE.2019.2935479>
- Nguyen N, Bera A, Mitra J (2018) Energy storage to improve reliability of wind integrated systems under frequency security constraint. *IEEE Trans Ind Appl* 54(5):4039–4047. <https://doi.org/10.1109/TIA.2018.2838558>
- Ying J, Yuan XM, Hu JB, He W (2018) Impact of inertia control of DFIG-based WT on electromechanical oscillation damping of SG. *IEEE Trans Power Syst* 33(3):3450–3459. <https://doi.org/10.1109/TPWRS.2018.2801283>
- Zhou X, Usman M, He P et al (2021) Parameter design of governor power system stabilizer to suppress ultra-low-frequency oscillations based on phase compensation. *Electr Eng* 103:685–696. <https://doi.org/10.1007/s00202-020-01101-8>
- Gururaja Rao HV, Prabhu N, Mala RC (2020) Wavelet transform-based protection of transmission line incorporating SSSC with energy storage device. *Electr Eng* 102:1593–1604. <https://doi.org/10.1007/s00202-020-00978-9>
- He JH, Chen KA, Li M, Luo YP, Liang CG, Xu Y (2020) Review of protection and fault handling for a flexible DC grid. *Protect Control of Mod Power Syst* 5(1):1–15. <https://doi.org/10.1186/s41601-020-00157-9>
- Gurung S, Jurado F, Naetiladnanon S et al (2019) Optimized tuning of power oscillation damping controllers using probabilistic approach to enhance small-signal stability considering stochastic time delay. *Electr Eng* 101:969–982. <https://doi.org/10.1007/s00202-019-00833-6>

14. He P, Qi P, Ji YQ, Li Z (2021) Dynamic interactions stability analysis of hybrid renewable energy system with SSSC. *Archiv Electri Eng* 70(2):445–462. <https://doi.org/10.24425/ae.2021.136995>
15. Dey P, Mitra S, Bhattacharya A, Das P (2019) Comparative study of the effects of SVC and TCSC on the small signal stability of a power system with renewables. *J Renew Sustain Energy* 11(3):033305. <https://doi.org/10.1063/1.5085066>
16. Sadiq AA, Buhari M, Adamu SS, Musa H (2020) Coordination of multi-type FACTS for available transfer capability enhancement using PI-PSO. *IET Gener Transm Distrib* 14(21):4866–4877. <https://doi.org/10.1049/iet-gtd.2020.0886>
17. Deng JC, Li C, Zhang XP (2015) Coordinated design of multiple robust FACTS damping controllers: a BMI-based sequential approach with multi-model systems. *IEEE Trans Power Syst* 30(6):3150–3159. <https://doi.org/10.1109/TPWRS.2015.2392153>
18. He P, Shen RJ, Wen FS, Pan Q (2021) Coordinated optimization of parameters of PSS and UPFC-PODCs to improve small-signal stability of a power system with renewable energy generation. *J Energy Eng* 147(2):04020089. [https://doi.org/10.1061/\(ASCE\)EY.1943-7897.0000737](https://doi.org/10.1061/(ASCE)EY.1943-7897.0000737)
19. Zhang GZ, Hu WH, Cao D, Yi JB, Huang Q, Liu Z, Blaabjerg F (2020) A data-driven approach for designing STATCOM additional damping controller for wind farms. *Int J Electr Power Energy Syst* 117:105620. <https://doi.org/10.1016/j.ijepes.2019.105620>
20. Bhukya J, Mahajan V (2021) Parameter tuning of PSS and STATCOM controllers using genetic algorithm for improvement of small-signal and transient stability of power systems with wind power. *Int Trans Electr Energy Syst* 31(7):e12912. <https://doi.org/10.1002/2050-7038.12912>
21. He P, Wen FS, Ledwich G, Xue YS (2016) An investigation on interarea mode oscillations of interconnected power systems with integrated wind farms. *Int J Electr Power Energy Syst* 78:148–157. <https://doi.org/10.1016/j.ijepes.2015.11.052>
22. Sloomweg JG, Kling WL (2003) The impact of large scale wind power generation on power system oscillations. *Electric Power Syst Res* 67(1):9–20. [https://doi.org/10.1016/S0378-7796\(03\)00089-0](https://doi.org/10.1016/S0378-7796(03)00089-0)
23. Yu GZ, Lin T, Zhang JN, Tian Y, Yang X (2019) Coordination of PSS and FACTS damping controllers to improve small signal stability of large-scale power systems. *CSEE J Power Energy Syst* 5(4):507–514. <https://doi.org/10.17775/CSEEJPES.2018.00530>
24. Haque MH (2004) Improvement of first swing stability limit by utilizing full benefit of shunt FACTS devices. *IEEE Trans Power Syst* 19(4):1894–1902. <https://doi.org/10.1109/TPWRS.2004.836243>
25. Karaagac U, Kocar I, Mahseredjian J, Cai LJ, Javid Z (2021) STATCOM integration into a DFIG-based wind park for reactive power compensation and its impact on wind park high voltage ride-through capability. *Electric Power Syst Res* 199:107368. <https://doi.org/10.1016/j.epsr.2021.107368>
26. Hasanvand H, Arvan MR, Mozafari B (2016) Coordinated design of PSS and TCSC to mitigate interarea oscillations. *Int J Electr Power Energy Syst* 78:194–206. <https://doi.org/10.1016/j.ijepes.2015.11.097>
27. Benabid R, Boudour M, Abido MA (2012) Development of a new power injection model with embedded multi-control functions for static synchronous series compensator. *IET Gener Transm Distrib* 6(7):680–692. <https://doi.org/10.1049/iet-gtd.2011.0296>
28. Pradhan AC, Lehn PW (2005) Frequency-domain analysis of the static synchronous series compensator. *IEEE Trans Power Deliv* 21(1):440–449. <https://doi.org/10.1109/TPWRD.2005.852311>
29. He P, Wen FS, Ledwich G, Xue YS, Wang KW (2013) Effects of various power system stabilizers on improving power system dynamic performance. *Int J Electr Power Energy Syst* 46:175–183. <https://doi.org/10.1016/j.ijepes.2012.10.026>
30. Kundur P, Balu NJ, Lauby MG (1994) *Power system stability and control*. McGraw-Hill, New York, pp 398–480

**Publisher's Note** Springer Nature remains neutral with regard to jurisdictional claims in published maps and institutional affiliations.

Springer Nature or its licensor (e.g. a society or other partner) holds exclusive rights to this article under a publishing agreement with the author(s) or other rightsholder(s); author self-archiving of the accepted manuscript version of this article is solely governed by the terms of such publishing agreement and applicable law.